Automatic glare removal in reflectance imagery of the uterine cervix

Holger Lange (Holger@STI-Medical.com)
STI Medical Systems, 733 Bishop Street, Suite 3100, Honolulu, Hawaii 96813, USA

ABSTRACT

Colposcopy is a diagnostic method used to detect cancer precursors and cancer of the uterine cervix. Computer-Aided-Diagnosis (CAD) for colposcopy is a new field in medical image processing. Colposcopists analyze glare (glint or specular reflection) patterns on the cervix to assess the surface contour (3D topology) of lesions, an important feature used to evaluate lesion severity. However, glare in the imagery presents major problems for automated image analysis systems. Glare eliminates all information in affected pixels and can introduce artifacts in feature extraction algorithms, such as acetowhite region detection. Although cross-polarization filters can be used to eliminate glare, the reality is that we have to deal with glare when we want to use existing cervical image databases or use an instrument that does not provide cross-polarized imagery. Here, we present the details and preliminary results of a glare removal algorithm for RGB color images of the cervix that can be used as a pre-processing step in CAD systems. The algorithm can be extended to multispectral and hyperspectral imagery. The basic approach of the algorithm is to extract a feature image from the RGB image that provides a good glare to background ratio, to detect the glare regions in the feature image, to extend the glare regions to cover all pixels that have been affected by the glare, and to remove the glare in the affected regions by filling in an estimate of the underlying image features. In our current implementation we use the green (G) image component as the feature image, given its high glare to background ratio and simplicity of calculation. Glare regions are either detected as saturated regions or small high contrasted bright regions. Saturated regions are detected using an adaptive thresholding method. Small high contrasted bright regions are detected using morphological top hat filters with different sizes and thresholds. The full extent of the glare regions is estimated by using a morphological constraint watershed segmentation to find the contour of the glare regions and adding a constant dilatation. The image features are estimated by interpolating the R,G,B color components individually from the surrounding regions based on Laplace's equation and modifying the intensity (I) component of the HSI color space transformed image. As the glare pattern is important to the physician, we embed it as a just visible intensity texture that does not affect the image processing. The performance of the algorithm is demonstrated using human subject data.

Keywords: Glare removal, glint, specular reflection, automated image analysis, uterine cervical cancer, colposcopy

1. INTRODUCTION

Uterine cervical cancer is the second most common cancer in women worldwide, with nearly 500,000 new cases and over 270,000 deaths annually[1,]. Colposcopy is the primary diagnostic method used in the US to detect cancer precursors and cancer of the uterine cervix, following an abnormal cytological screen (Papanicolaou smear). A colposcopic examination involves a systematic visual evaluation of the lower genital tract (cervix, vulva and vagina), with special emphasis on the subjective appearance of metaplastic epithelium comprising the transformation zone on the cervix[2]. For this purpose an optical colposcope is used, which has been in use for almost 80 years. A colposcope is a low powered binocular microscope with a built in white light source and objective lens attached to a support mechanism. A 3-5% acetic acid solution is applied, causing abnormal and metaplastic epithelia to turn white. Cervical cancer precursor lesions and invasive cancer exhibit certain distinctly abnormal morphologic features that can be identified by colposcopic examination. Lesion characteristics such as margin; color or opacity; blood vessel caliber, intercapillary spacing and distribution; and contour are considered by physicians (colposcopists) to derive a clinical diagnosis[3]. These colposcopic signs, when considered aggregately, determine the severity of the neoplasia and discriminate abnormal findings from similarly appearing, anatomically normal variants.

The digital revolution in medical imaging is on its way, enabling more and more the use of sophisticated computer programs to assist the physicians with their diagnoses – Computer-Aided-Diagnosis (CAD). Examples of existing CAD systems can be seen in applications like mammography, chest-lung node detection and virtual colonoscopy[4]. Clinicians and academia have suggested and shown proof of concept to use automated image analysis of

cervical imagery for cervical cancer screening and diagnosis [5.,6.,7.,8]. STI Medical Systems is developing such a Computer-Aided-Diagnosis (CAD) system for colposcopy – ColpoCAD™ [9].

Colposcopists analyze glare (glint or specular reflection) patterns on the cervix to assess the surface contour (3D topology) of lesions, an important feature used to evaluate lesion severity. However, glare in the imagery presents major problems for automated image analysis systems. Glare eliminates all information in affected pixels and can introduce artifacts in feature extraction algorithms, such as acetowhite region detection. Although cross-polarization filters can be used to eliminate glare, the reality is that we have to deal with glare when we want to use existing cervical image databases or use an instrument that does not provide cross-polarized imagery.

We conducted a technology exploration project for the development of a CAD system for colposcopy, prototyping image processing algorithms for glare removal, anatomic features detection, acetowhite region detection, lesion margin shape analysis, and blood vessel mosaic and punctuation structure detection using RGB images from 111 human subjects participating in a clinical study of our Hyperspectral Diagnostic Imaging (HSDI™) instrument[10,11]. Here, we present the details and preliminary results of the glare removal algorithm for single RGB color images of the cervix that can be used as a pre-processing step in CAD systems. The algorithm can be extended to multispectral and hyperspectral imagery.

Should the data set include stereoscopic images or an image sequence, then those images could be registered spatially to each other and the regions affected by the glare in one image could be retrieved from another image where the corresponding region is not affected by glare.

2. ALGORITHM DESCRIPTION

The image processing algorithm described in this paper detects and removes the glare in RGB (Red-Green-Blue color space) images taken from an uterine cervix. We developed this algorithm using RGB images from 111 human subjects. The input image for the algorithm is a RGB image from a uterine cervix, as shown in figure 1. The basic approach of the algorithm is to extract a feature image from the RGB image that provides a good glare to background ratio, to detect the glare regions in the feature image, to extend the glare regions to cover all pixels that have been affected by the glare, and to remove the glare in the affected regions by filling in an estimate of the underlying image features. Those four steps are described in detail in the following paragraphs. The output of the algorithm is a binary mask identifying the detected glare regions and the glare removed RGB image, as shown in figure 8.

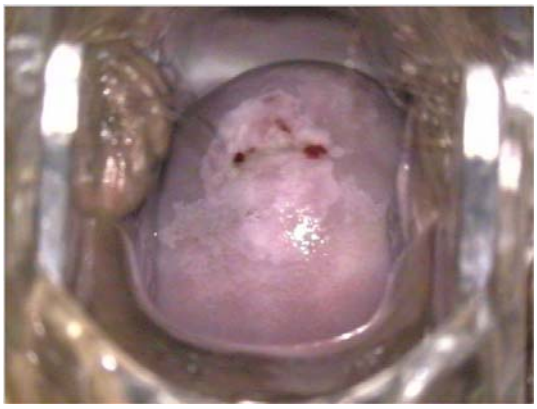

Figure 1: Original RGB image of the uterine cervix.

2.1 Glare Pixel Feature Extraction

The goal of the glare pixel feature extraction is to calculate a feature image from the original RGB image that provides a high glare to background ratio in order to improve the detection of the glare regions. Glare can be characterized by high contrast or saturated intensity and a white color. The background of the glare, the cervix, can be characterized by a reddish or pinkish color, but also white color for whitened regions after the application of acetic acid to the cervix. A glare pixel feature could be calculated as a function of high intensity and low color saturation. There are different ways of combining the intensity and the color saturation (e.g. multiplication, subtraction), as well as calculating the intensity and color saturation (e.g. ratio, subtraction) based on the original R, G, B values or their min, max and mean functions.

Two ways to calculate a glare pixel feature image are shown in equations 1 and 2. Based on the Hue-Saturation-Intensity (HSI) color space, the intensity is calculated as the mean, and the color saturation is based on the ratio of the min over the mean (equation 1). A modification of this can be derived from the observation that a higher glare to background ratio can be obtained by using the min instead of the mean for the intensity calculation and using the max instead of the mean for the color saturation calculation (equation 2). The min, mean and max are the same for a glare region, because of the white color - meaning that all colors R, G, B are the same. The background typically is colored and therefore the min, mean and max are different. For the intensity calculations, the min is smaller than the mean, providing a higher glare to background ratio. For the color saturation calculations, the max is higher than the mean, providing a higher glare to background ratio. The background characteristics suggest that green (G) could be used to approximate the min and red (R) could be used to approximate the max. Figure 2 shows a simplified illustration of the typical R, G, B, 1D profiles for the background and the glare.

$$Glare = I*(1-S), \qquad I = mean(R,G,B), \qquad S = \frac{\min(R,G,B)}{mean(R,G,B)} \qquad \text{Equation 1}$$

$$Glare = I - S, \qquad I = \min(R,G,B), \qquad S = \frac{\min(R,G,B)}{\max(R,G,B)} \qquad \text{Equation 2}$$

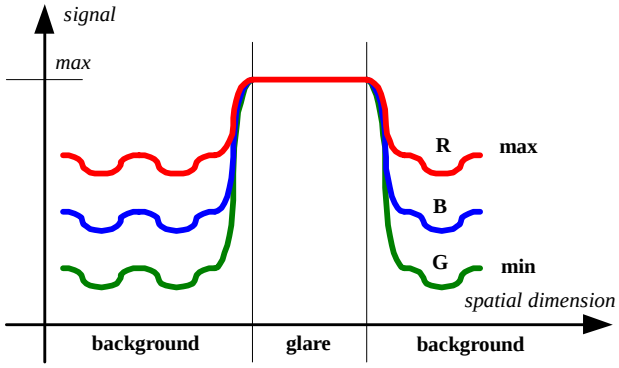

Figure 2: Simplified illustration of the typical R,G,B 1D profiles of the background and the glare.

The glare detection and removal algorithm was tested with different ways of calculating the glare pixel feature, including the green channel and equation 1 and 2. The conclusion was to use the green (G) image component as the glare pixel feature because it provides a good glare to background ratio and does not require any computation. There was no degradation in the glare region detection performance noticed in the cervix region of interest when compared to the other ways of calculating the glare feature images. Figure 3 shows different glare feature images in a negative image presentation for better human perception. The extension to multispectral and hyperspectral imagery is done by replacing the R,G,B channels in equation 1 and 2 with the multispectral or hyperspectral channels. Most likely a channel with a wavelength close to the green color will provide similar results.

a. 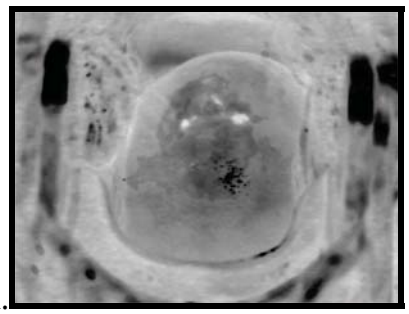 b. 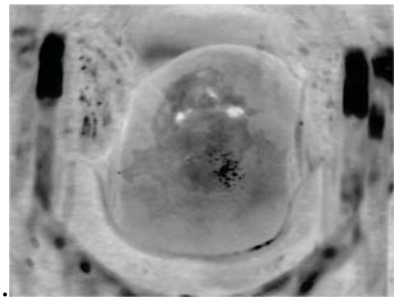 c. 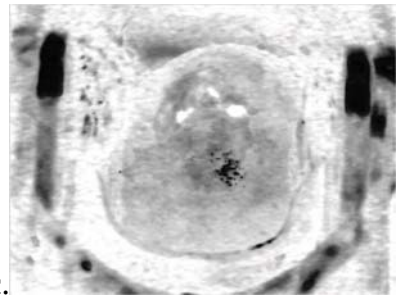

Figure 3: Different glare pixel feature images shown as negative images – a. Green, b. Equation 1, c. Equation 2.

2.2 Glare Region Detection

Glare regions are detected as saturated regions and small high contrasted regions. The saturated regions are detected by applying an adaptive threshold to the glare pixel feature image. The algorithm is based on the assumption that an image with glare regions produces a histogram with a local maximum at saturated values. The assumption is verified for each image. The value of the adaptive threshold is determined by the maximum position of the local minima in the histogram. The glare pixel feature image is then thresholded to provide a binary image highlighting the pixels belonging to saturated regions. The histogram is calculated from the glare pixel feature image and smoothed using an Alternating Sequential Filter (Closing followed by Opening). The regional local maxima in the histogram are extracted using a Watershed operation. For the case that the maximum is at the highest histogram position the histogram is extended by one position with a zero value. The maximum position of those maxima is then compared to a threshold to verify that there is a local maximum at saturated values. If this test fails no saturated regions will be detected and a zero image will be output. The regional local minima in the histogram are extracted using a Watershed operation on the negative histogram. The adaptive threshold is determined as the maximum position of the minima. The thresholding uses the adaptive threshold and outputs a binary image of the pixels belonging to saturated regions. Figure 4a shows the detected saturated pixels overlaid on the glare pixel feature image. We assume that large glare regions have some saturated pixels and will be detected using the saturated region detection algorithm. Small glare regions, on the other hand, may not exhibit saturated pixels but rather exceptionally high contrast. We detect small, high contrasted, bright regions using the union of a "Open Top Hat with Reconstruction" operation filter bank with different box structuring element sizes, and different corresponding thresholds. Only small, high contrasted, bright regions above an absolute threshold are considered. The absolute threshold is determined to be a certain percentage between the mean and the maximum values of the glare pixel feature image. Figure 4b shows the detected small bright regions overlaid on the glare pixel feature image. Note that in consecutive image processing steps we are looking for bright white regions (white due to the effect of acetic acid), and that therefore it would not be wise to detect and remove general high contrasted bright regions as glare. The union of the saturated and small bright regions represents the totality of the detected glare regions.

a. 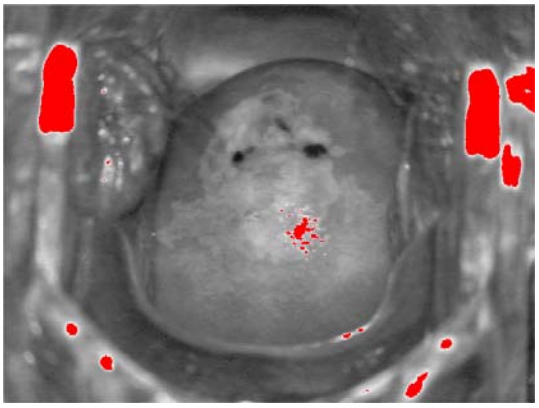 b. 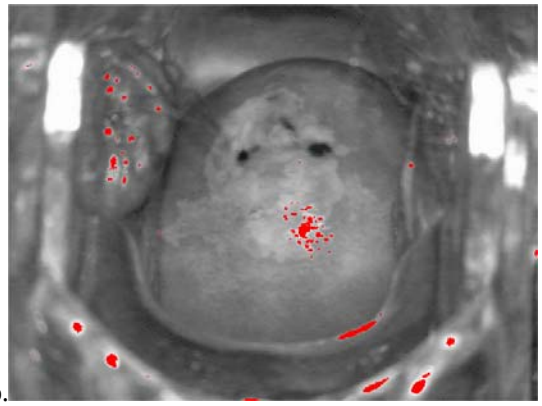

Figure 4. a. Saturated regions overlay, b. Small bright regions overlay.

2.3 Glare Region Extension

The goal is to provide an extension of the glare regions to the point that the glare does not influence the surroundings outside the regions. This is required because the following glare region removal step interpolates the glare regions from their surrounding regions that then should not include any effect from the glare. Figure 5 shows a simplified illustration of the impact of the glare region extent on the interpolation of the RGB color components. The extension of the glare regions is done in two steps: first, using a morphological constraint watershed segmentation algorithm, the glare regions are extended to the steepest point on the edge of the glare, the contour, see figure 5a and 6a.; second, a constant dilatation is applied to the glare regions, see figure 5b and 6b. The constrained Watershed segmentation algorithm works on the gradient of the glare pixel feature image using the detected glare regions and (union) background markers. The background markers are obtained by detecting the regional minima of the gradient of the glare pixel feature image after basins of a certain height have been eliminated, reducing the influence of the noise in the image. In order to make sure that the background markers are not connected to the glare and thereby being able to extend the glare markers (e.g. high intensity/contrasted crest leading into a glare), the background markers are intersected with the negative image of

the dilated glare regions. Using the watershed segmentation regions, the region segments containing glare are extracted. The extension (red) of the glare regions (green) by the watershed segmentation is shown in figure 6a. The constant dilatation of the contour extended glare regions provides the final extended glare regions shown in 6b. Note that the extension of the glare regions using a constant dilatation is not accurate and can be improved using more sophisticated approaches that analyze the surroundings of the glare regions.

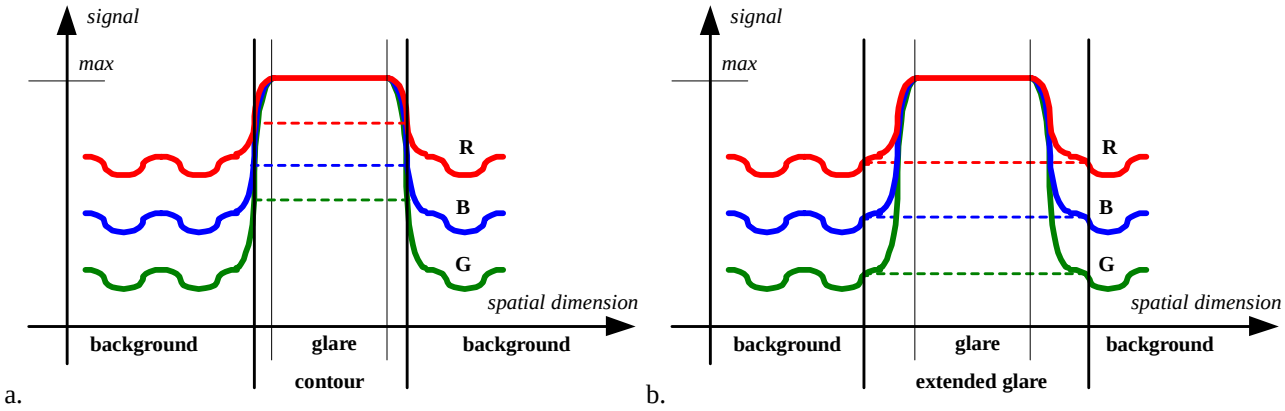

a. b.

Figure 5: Impact of the glare region extent on R,G,B color interpolation.

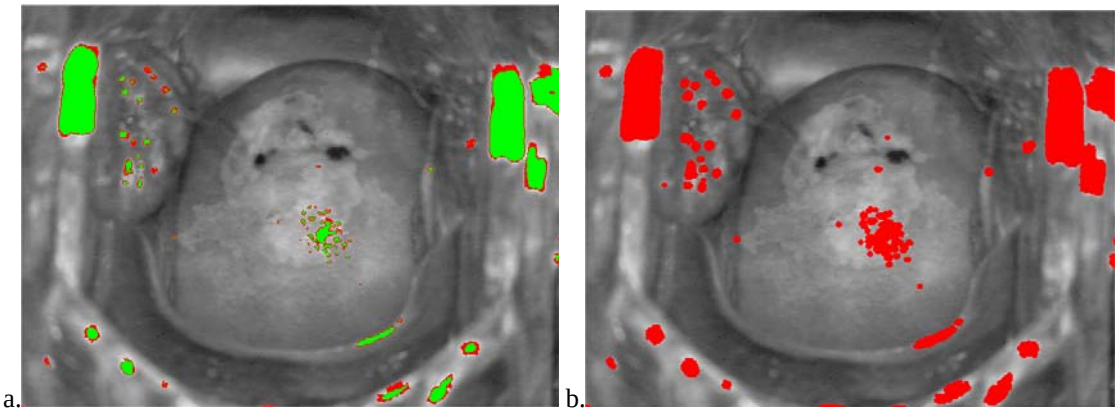

a. b.

Figure 6: a. Glare regions (green) contour extension (red) overlay, b. Constant dilatation extension overlay.

2.4 Glare Region Removal

The glare regions are removed by filling in the affected pixels with an estimate of the underlying image features. The image features are estimated by interpolating the R,G,B color components individually from the surrounding regions based on Laplace's equation and modifying the intensity (I) component of the HSI color space transformed image. Figure 7 shows the interpolated RGB image. Note that the interpolated RGB image lost most texture features in the interpolated region (smooth interpolation). More sophisticated approaches that detect the texture features (like contours) surrounding the regions and use them for the interpolation could improve the texture feature in the glare regions. Note that the regions containing glare lost all information of the underlying real image features (without glare), therefore those features can only be estimated but not truly retrieved. To some extent the glare removal represents a "best" guess of what the hidden image features in the glare regions could have been. We recognize that the glare pattern does not correspond to the underlying texture feature, but as it is important to the physician, we embed it as a just visible intensity texture that does not affect the image processing. We transform the original image and the interpolated image from the RGB to the HSI color space. We add the glare pattern as an intensity texture feature to the image by adding to the interpolated intensity function a scaled , just visible, fused (union) intensity function of the error function between the interpolated intensity and the original intensity and the binary glare regions. The scale is fixed to a low visible contrast for humans. All regions get scaled independently. The resulting HSI image is then color transformed back into a RGB image including the intensity texture. Figure 8a shows the glare regions and 8b shows the final glare removed RGB image. The R,G,B color interpolation can be extended to multispectral and hyperspectral imagery by interpolating

each channel individually. Embedding an intensity texture requires the existence of a color space transformation into a color space that includes the intensity function. We can limit the application of the glare removal to the cervix region only, which might provide a “nicer” image to look at for the physician, by using a mask that outlines the cervix region. The cervix region mask can be provided automatically by our cervix region detection algorithm. Figure 9a shows the cervix region mask and 9b the results of the glare removal when limited to the cervix region.

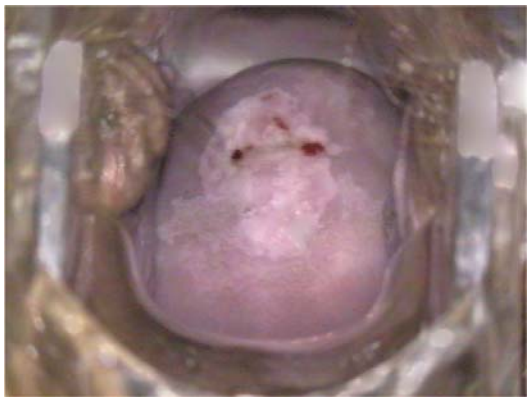

Figure 7: Interpolated RGB image.

a. 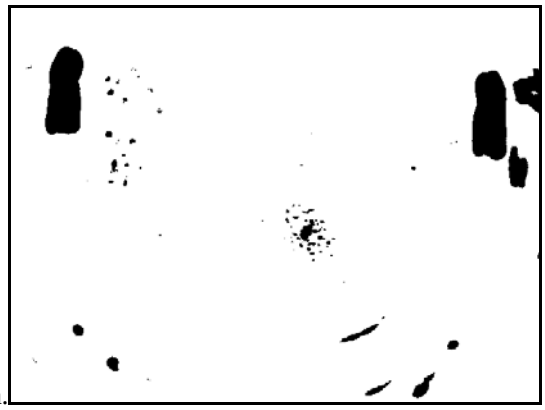 b. 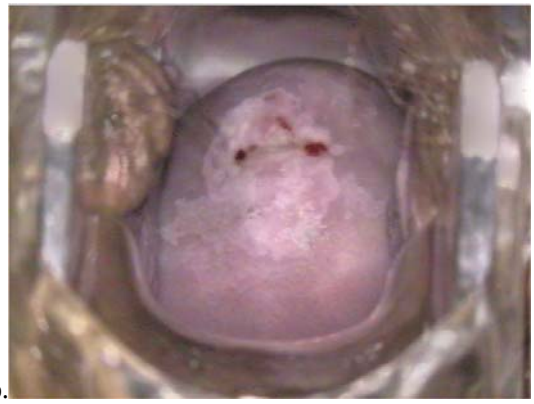

Figure 8: a. Glare mask, b. Glare removed RGB image.

a. 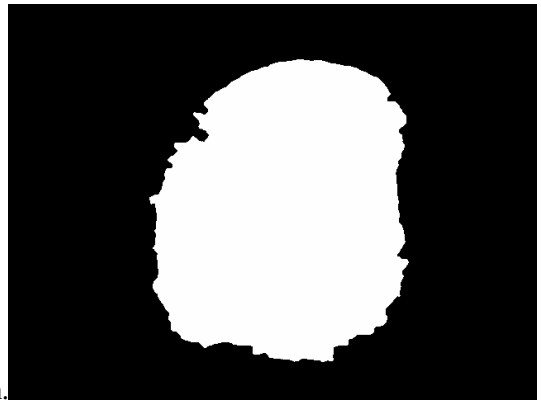 b. 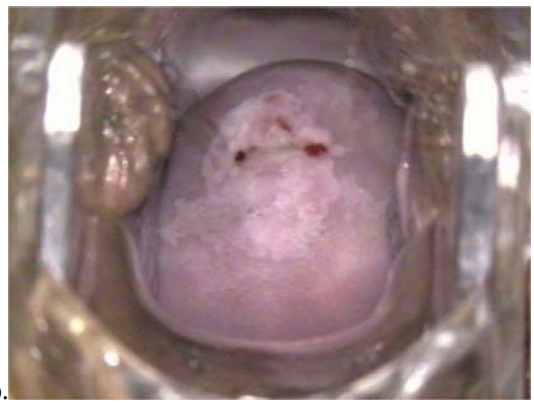

Figure 9: a. Cervix region mask, b. Glare removed on cervix region only.

3. PRELIMINARY RESULTS

In our technology evaluation project, we used RGB images from 111 human subjects for the development of the glare removal algorithm. The algorithm performance was assessed by qualitative subjective inspection of the processed images. The performance of the glare removal algorithm can be assessed by looking at the preliminary results shown in figure 10. Note that we focus only on the cervix region, for that is the only part of the image that will be analyzed by image analysis algorithms in a CAD system, and therefore requires the glare removal.

Qualitatively, the algorithm shows a very good performance over the entire data set. All the regions with glare seem to be properly detected and removed. The color properties seem to be approximated correctly. The intensity texture seems to be reasonably well reconstructed.

Testing with constructed test cases revealed possible shortcomings of the algorithm, which actually have not been encountered in our human subject data set:
a. When the glare is located on a white region in the image with a dark background and the glare regions cover most of the surface of the white regions, then the entire white region might get removed.
b. When the glare region is on a color contour and the glare is more on one region than on the other, the color from the smaller region gets propagated too far into the other larger region - the colors are spreading out.

The quantitative performance of the glare removal algorithm will be assessed as part of our ColpoCAD™ development. STI Medical Systems currently acquires a data set of images with and without glare (cross-polarization). The images without glare will provide the "ground truth" for the glare removal algorithm and be used for a quantitative assessment. Once we have a full functional ColpoCAD™ system we will also assess the performance impact of the glare removal algorithm on the overall system performance.

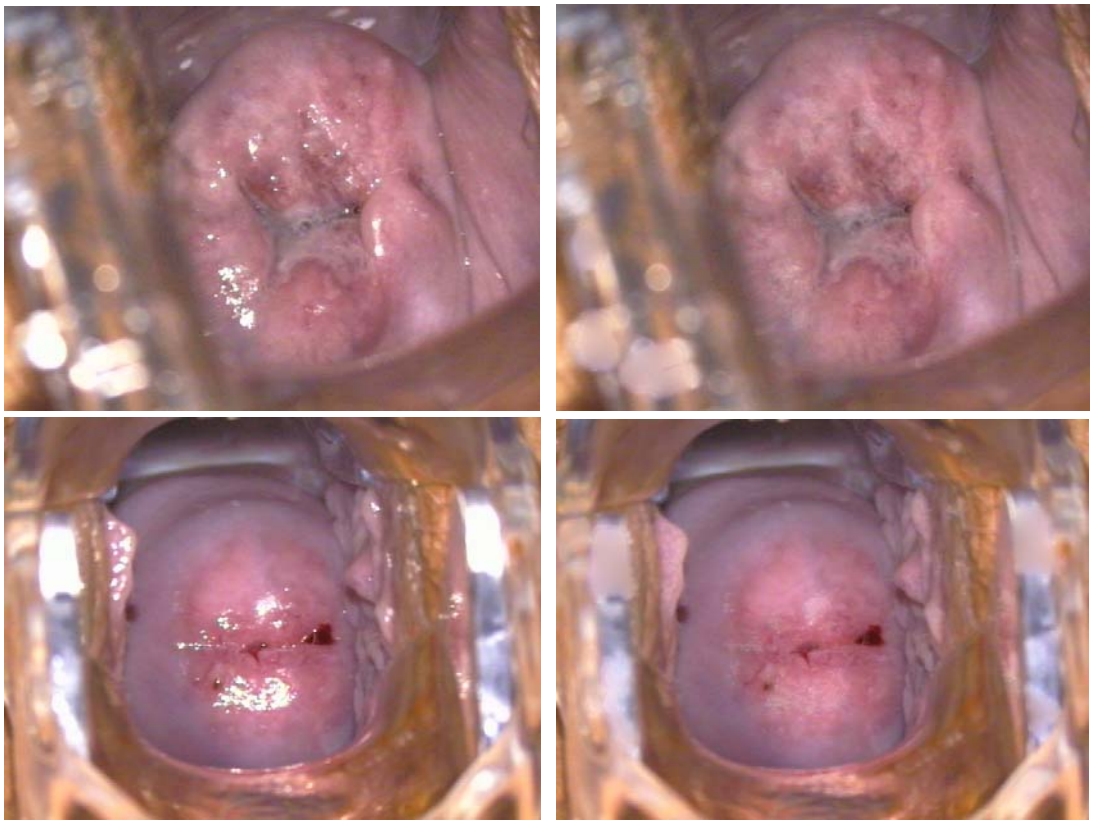

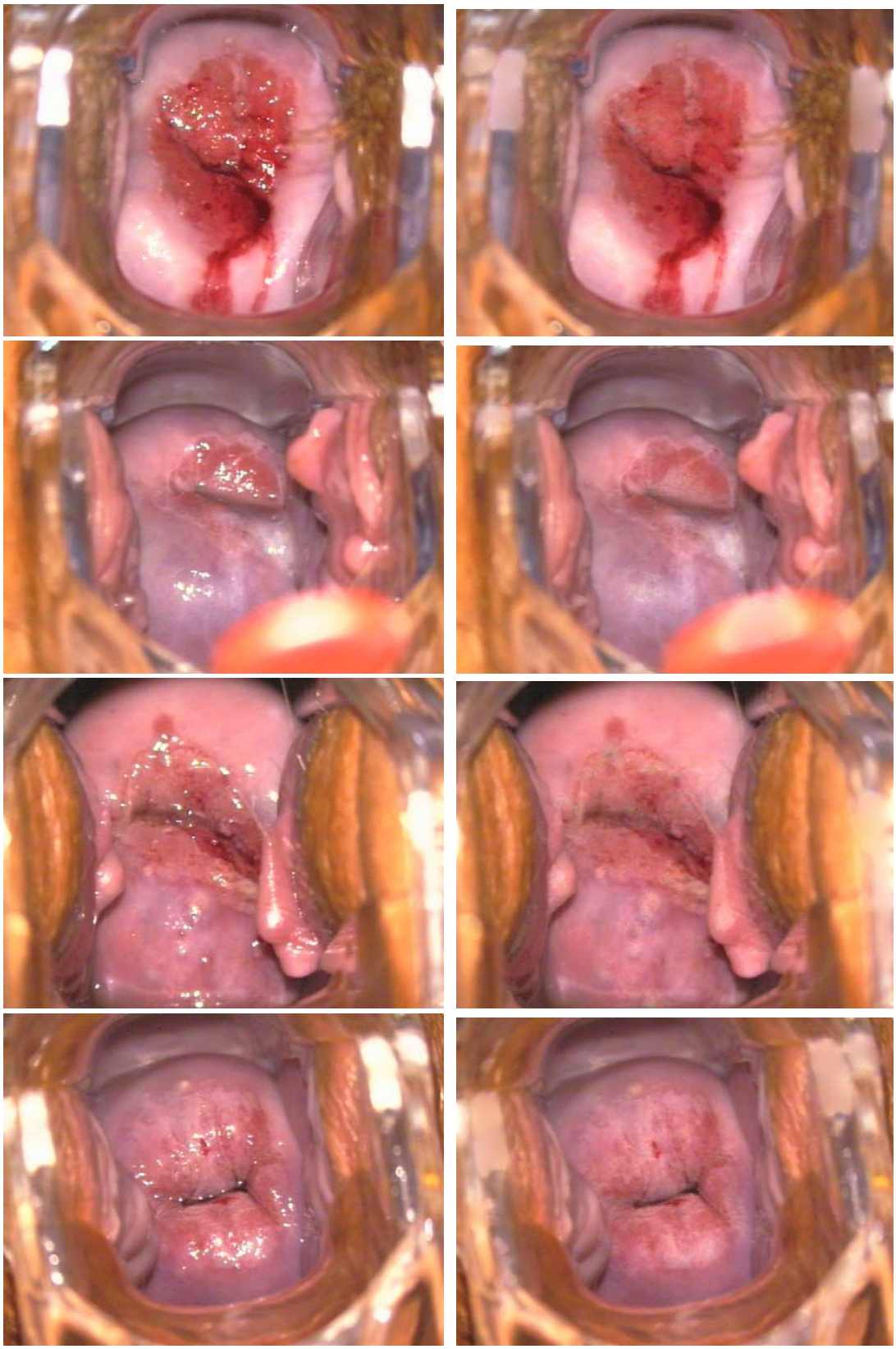

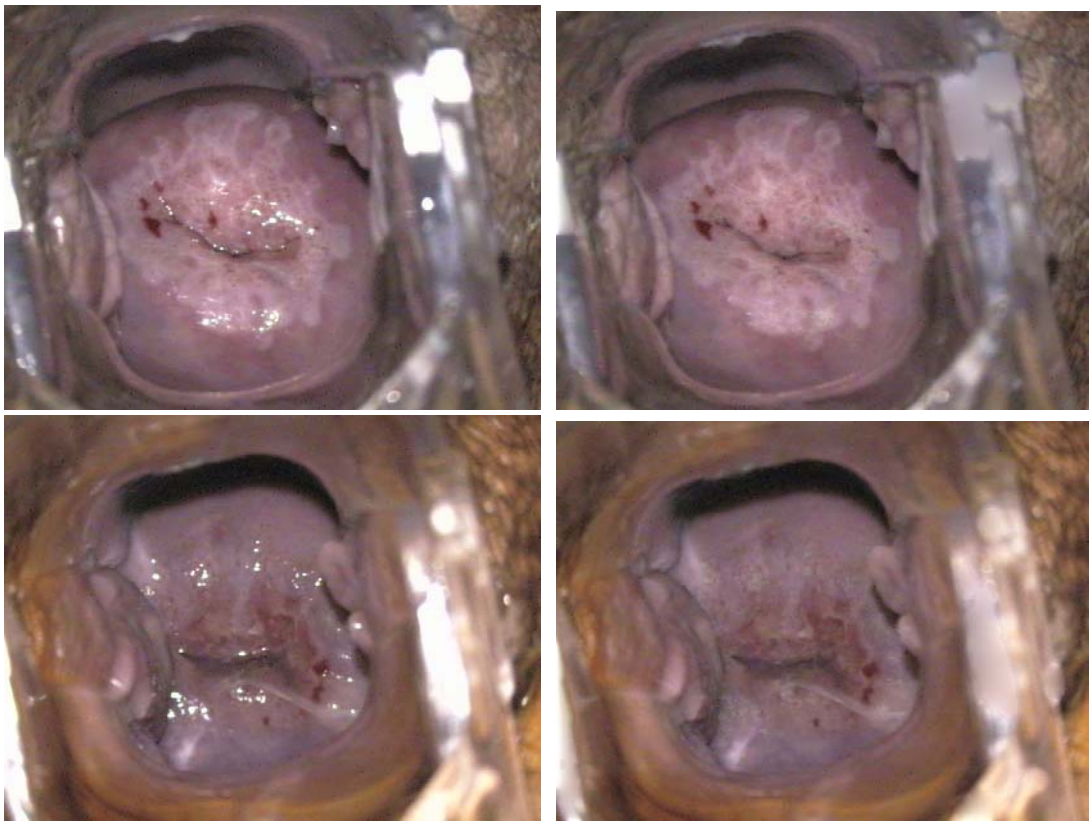

Figure 10: Preliminary results of the glare removal algorithm.

4. CONCLUSIONS

We presented the details and preliminary results of a glare removal algorithm for RGB color images of the uterine cervix that can be used as a pre-processing step in Computer-Aided-Diagnosis (CAD) systems for colposcopy. We used RGB images from 111 human subjects for the development of the glare removal algorithm. Our qualitative assessment of the algorithm over the entire data set indicates a very good performance. The quantitative performance of the glare removal algorithm will be assessed as part of our ColpoCAD™ development, when we will compare the glare removal results against the "ground truth" given by corresponding glare free images (cross-polarized) and assess the performance impact of the glare removal algorithm on the overall system performance of the CAD system.

5. ACKNOWLEDGMENTS

We would like to thank the following institutions for their support and collaboration in advancing this technology: Tripler Army Medical Center, Honolulu, Hawaii; Lund University Medical Laser Centre, Lund, Sweden; and the Laser Surgery Department, Vilnius University, Vilnius, Lithuania.

REFERENCES

[1] http://www-depdb.iarc.fr/globocan2002.htm

[2] B.S. Apgar, Brotzman, G.L. and Spitzer, M., Colposcopy: Principles and Practice, W.B. Saunders Company: Philadelphia, 2002

[3] Reid R, Scalzi P. Genital warts and cervical cancer. VII An improved colposcopic index for differentiating benign papillomaviral infection from high-grade cervical intraepithelial neoplasia. Am J Obstet Gynecol 1985;153:611-618

[4] Frost & Sullivan; Market Research; U.S. Computer Aided Detection (CAD) Markets – An Analysis of an Emerging Market; June 23, 2003

[5] Craine BL, Craine ER. Digital imaging colposcopy; basic concepts in applications. Obstet Gynecol 1993;82:69-73

[6] Eillen D. Dickman, Theodore J. Doll, Chun Kit Chiu, and Daron G. Ferris, Identification of Cervical Neoplasia Using a Simulation of Human Vision, Journal of Lower Genital Tract Disease, Vol. 5, No. 3, 2001, pp144-152
[7] Mikhail MS, Merkatz IR, Rommey SL. Clinical usefulness of computerized colposcopy: Image analysis and conservative management of mild dysplasia. Obstet Gynecol 1992;80:5-8
[8] Mikhail MS, Romney SL. Computerized measurement of intercapillary distance using image analysis in women with cervical intraepithelial neoplasia: correlation with severity. Obstet Gynecol 2000;95:52-3
[9] Lange H. and Ferris, Daron G.; Computer-Aided-Diagnosis (CAD) for colposcopy; SPIE Medical Imaging 2005; SPIE Proc. 5747, 2005
[10] Gustafsson U., McLaughlin E., Jacobson E., Håkansson J., Troy P., DeWeert M., Pålsson S., Soto Thompson M., Svanberg S. , Vaitkuviene A., and Svanberg K.; Fluorescence and reflectance monitoring of human cervical tissue in vivo -a case study; SPIE Photonics West Biomedical Optics (BiOS) 2003; SPIE Proc. 4959, 2003
[11] Gustafsson U., McLaughlin E., Jacobson E., Håkansson J., Troy P., DeWeert M., Pålsson S., Soto Thompson M., Svanberg S. , Vaitkuviene A., and Svanberg K.; In vivo fluorescence and reflectance imaging of human cervical tissue; SPIE Medical Imaging 2003; SPIE Proc. 5031, 2003